## Title
Increasing the thermoelectric figure of merit of tetrahedrites by Co-doping with nickel and zinc



## Journal
Chemistry of Materials, 27(2)

## ISSN
0897-4756

## Authors
Lu, X
Morelli, DT
Xia, Y
et al.

## Publication Date
2015-01-27

## DOI
10.1021/cm502570b

# Increasing the Thermoelectric Figure of Merit of Tetrahedrites by Co-doping with Nickel and Zinc

Xu Lu[1], Donald T. Morelli[1,2,*], Yi Xia[3], and Vidvuds Ozolins[3]

[1]Department of Physics & Astronomy, Michigan State University, East Lansing, Michigan 48824 USA

[2]Department of Chemical Engineering & Materials Science, Michigan State University, East Lansing, Michigan 48824 USA

[3]Department of Materials Science & Engineering, University of California-Los Angeles, Los Angeles, California 90095 USA

**ABSTRACT:** We report a more than 30% increase in the thermoelectric figure of merit of Ni-doped tetrahedrite ($Cu_{12}Sb_4S_{13}$) by the addition of Zn. We show that this enhancement is due to the combination of two effects: 1) a tuning of the Fermi energy to optimize the Seebeck coefficient and thermoelectric power factor; and 2) a reduction in thermal conductivity due to decreases in both the electronic and lattice thermal conductivities. Unlike tetrahedrites doped solely with Zn, which can become electrically insulating at high Zn concentrations, Ni doped samples remain conducting due to the existence of an additional valence band from spin-split Ni states. By adding Zn to these Ni-doped materials, electrons can fill the holes in the valence band, allowing for tuning of the thermoelectric properties. Tetrahedrites optimally doped with both Ni and Zn have thermal conductivity approaching theoretical minimum values, which helps boost the thermoelectric figure of merit $zT$ in these compounds above unity.

## INTRODUCTION

Thermoelectric (TE) materials with low cost and high performance are currently under intensive study due to their potential large-scale application in waste heat recovery in the power-producing, processing, and automobile industries. TE materials function by converting thermal energy to electrical energy using the Seebeck effect. The performance of TE materials is evaluated by the figure of merit $zT=S^2\sigma T/\kappa$, where $S$ is the Seebeck coefficient, $\sigma$ the electrical conductivity, $T$ the absolute temperature, and $\kappa$ thermal conductivity. Commercial TE materials typically display maximum values of $zT$ on the order of unity. A major obstacle in the development of TE materials with high $zT$ is the "contra-indicated" nature of the combination of properties entering the figure of merit; achieving, for instance, high electrical conductivity and low thermal conductivity, or high electrical conductivity and large Seebeck coefficient, in a single material. Many new approaches have been implemented recently to overcome this contra-indicated nature, most notably the concept of phonon-glass/electron-crystal[1], and, more recently, the careful design of hierarchically-structured nanocomposites[2]. While such approaches have met with considerable success in raising the value of $zT$ significantly above unity, often the compounds created are comprised of rare or toxic elements, calling into question their use in large scale waste heat recovery applications. Recently, binary copper semiconductors $Cu_xS$ and $Cu_xSe$ have been revisited as potential highly efficient thermoelectric materials, and have been claimed to have $zT$ values as high as 1.5, a value partly ascribed to the liquid-like substructure of the copper ions[3], although they suffer from well known issues related to copper ion diffusion[4].

An earth-abundant natural mineral-based compound family, tetrahedrites of nominal composition $Cu_{12-x}(Zn, Fe, Ni, Mn)_xSb_4S_{13}$, has recently been found to display high performance thermoelectric properties[5-8]. The highest $zT$ values reported for Zn and Ni doped tetrahedrites are 0.9 and 0.7, respectively. Tetrahedrites are semiconductors[5] with electronic band gap of approximately 1.2 eV and

large Seebeck coefficient. The complex crystal structure[9] (Figure 1, left panel) features two distinct Cu sites: Cu (1), in which copper atoms are tetrahedrally coordinated by S; and, more unusually, Cu(2), with copper atoms trigonally-coordinated by S (Figure 1, center panel). In this latter arrangement the Cu atoms have been shown to undergo

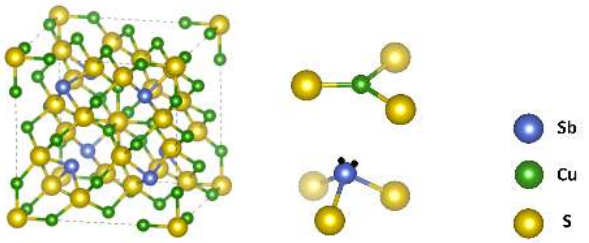


Figure 1. The tetrahedrite crystal structure (left). Two prominent features thought to play a role in strong anharmonicity and low lattice thermal conductivity are the trigonal-planar Cu atoms, which exhibit large dynamic displacement (top right), and the trigonally-coordinated Sb atoms, which harbor lone pair electrons (indicated here with small black dots).

large dynamic displacement[6]. Additionally, Sb atoms are trigonally-coordinated with S and harbor $s^2$ lone pairs (Figure 1, right panel). The atomically displaced Cu(2) atoms and the Sb lone pair arrangement have both recently been identified[6,10] as favoring strong lattice anharmonicity and low lattice thermal conductivity. In addition, TE materials of this family synthesized directly from the natural mineral itself display both high figure of merit[11,12] and good mechanical properties[13], showing promise for large-scale applications. Here, we report our efforts to improve the thermoelectric properties of tetrahedrite compounds by Ni and Zn co-doping.

Both experimental and theoretical results[5,6] show that Zn and Ni doping have different effects on the electronic structure of these compounds. Since undoped $Cu_{12}Sb_4S_{13}$ is a metal-like heavily doped *p*-type semiconductor with the Fermi level below the top of the valence bands, Zn doping provides extra electrons to fill the holes in the valence band, moving the Fermi level into the energy gap. Since undoped $Cu_{12}Sb_4S_{13}$ has two empty hole states per formula unit, $Cu_{10}Zn_2Sb_4S_{13}$ is almost insulating, but for Zn substitutions ≤ 2 the properties may be tuned to provide for large $zT$. On the other hand, Ni doped tetrahedrites are still conducting at $x$ = 2 and achieve their highest $zT$ at $x$ = 1.5. In this work, we further tune the properties of this optimally Ni-doped tetrahedrite by the addition of Zn. In a series of compounds of compositions $Cu_{10.5}Ni_{1.5-x}Zn_xSb_4S_{13}$ ($x$ = 0, 0.2, 0.5, 1) we demonstrate that the power factor ($PF=S^2\sigma$) remains unchanged for light Zn doping ($x$=0.2 and 0.5), but the lattice thermal conductivity is reduced by 25% for $x$ = 0.5 at 723 K, and approaches the theoretical minimum lattice thermal conductivity. As a result, the $zT$ values for these compounds rise above unity, a greater than 30% enhancement over that of the best pure Ni-doped samples.

## EXPERIMENTAL AND COMPUTATIONAL SECTION

**Materials synthesis.** $Cu_{10.5}Ni_{1.5-x}Zn_xSb_4S_{13}$ samples were synthesized by a direct melting method. The starting elements- Cu shots (99.99 %, Alfa-Aesar), Sb and Zn shots (99.9999 %, Alfa-Aesar), and S and Ni pieces (99.999%, Alfa-Aesar) - were weighed out in stoichiometric proportions and then placed into quartz ampoules. The ampoules were evacuated by a turbo molecular pump to a pressure of $<10^{-5}$ Torr and then sealed by an oxygen/methane torch. The sealed ampoules were suspended in a vertical tube furnace, heated at the rate of 0.3 K $min^{-1}$ to 923 K and kept at that temperature for 12 hours. Finally, the furnace was slowly cooled at the rate of 0.4 K $min^{-1}$ to room temperature.

**Sample preparation.** The crushed ingots were placed into a stainless jar for 5 minutes of ball milling in a SPEX Sample Prep 8000M machine. The product powders were cold pressed and put back to ampoules in a box furnace for annealing for one week at 723 K. The annealed pellets were ball milled for another 30 minutes with the ball milling jar back-filled with argon. The fine powders were then loaded under argon into a graphite die with diameter of 10 mm and hot-pressed for 30 minutes at 723 K and 80 MPa. All the hot pressed pellets were single phase tetrahedrite and in excess of 98 % of theoretical density. X-ray diffraction patterns and lattice parameter information for select samples are shown in Figures S1 and S2 of the Electronic Supplementary Information (ESI). It has been established in literature[9] that metal substitutions for Cu occupy the Cu(1) site. The pellets were then cut using a diamond saw into 3 mm*3 mm*8 mm bars and 10 mm diameter*1.5 mm thickness disks for electrical transport and thermal conductivity measurements, respectively.

**Thermoelectric measurements.** Electrical transport properties were measured using an Ulvac ZEM-3 system from room temperature to 723 K. The thermal conductivity was calculated from the product of the thermal diffusivity (measured using a Netzsch LFA 457 laser flash system), heat capacity, (measured using a Netzsch DSC200F3 differential scanning calorimeter) and density (measured using the Archimedes method). We estimate that the uncertainties in our electrical and thermal transport measurements are 5 % and 10 %, respectively.

**Density-functional theory (DFT) calculations.** The projector-augmented wave (PAW) method as implemented in the highly efficient Vienna *Ab Initio* Simulation Package (VASP)[14-17] was used to perform structural relaxations and to calculate electronic band structures and densities of states. Self-consistent spin-polarized calculations were performed using the Perdew-Becke-Ernzerhof (PBE)[18,19] generalized gradient approximation (GGA) for the exchange-correlation (xc) functional and plane wave basis with the cutoff energy of 450 eV. Calculations were performed using the primitive cell of $Cu_{12}Sb_4S_{13}$ and electronic Bloch functions were calculated on regular Monkhorst-pack **k** point meshes of 10×10×10. Structures for $Cu_{11}Ni_1Sb_4S_{13}$ and $Cu_{11}Ni_2Sb_4S_{13}$ were obtained via picking the lowest-energy configuration among all symmetry-

inequivalent substitutions on Cu sites after fully relaxing all structural degrees of freedom. Relaxation was stopped when all forces were below 0.02 eV/Å and stresses below 0.5 kbar.

## RESULTS AND DISCUSSION

**Band Structure of Ni-doped tetrahedrite.** The electronic band structures and densities-of-states (DOS) of pure $Cu_{12}Sb_4S_{13}$ and Zn-doped $Cu_{10}Zn_2Sb_4S_{13}$ were calculated previously.[5] Atom-decomposed electronic density-of-states (eDOS) of pristine $Cu_{12}Sb_4S_{13}$ is shown in Figure S3 of the ESI. Its main feature relevant for the thermoelectric properties is a valence band complex that is formed by hybridizing S 3*p* and Cu 3*d* orbitals. The pure compound has a well-developed energy gap separating the *p-d* hybridized valence bands from the conduction bands of predominantly S and Sb *p* character (see Figure S3 of ESI). Since the Fermi level resides below the top of the valence band complex, the material can be best described as an almost metallic heavily doped *p*-type semiconductor. It has two unfilled holes per formula unit due to the presence of an "extra" $S^{2-}$ ion in the octahedral 2*a* site; sulfur here is energetically stabilized by strong covalent bonding with the *s* and *d* orbitals of the surrounding three-fold coordinated $Cu^+$ ions on the 12*e* sites. These hybridized states show up as sharp peaks in the S *p* and Cu *s* and *d* partial eDOS curves at the bottom of the valence band complex in Figure S3 of ESI. With substitution of two Zn atoms for Cu, the extra Zn *4s* electrons fill the valence band holes, the Fermi level moves into the band gap, and the material becomes insulating; this has been confirmed previously by experiments.[5]

The behavior with Ni doping, however, is quite different. Using DFT calculations, we find that Ni prefers to substitute for Cu on the tetrahedral 12*d* sites. Our DFT band structure results for the Ni-doped compound $Cu_{11}Ni_1Sb_4S_{13}$ are shown in Figure 2; similar plots are shown for the double-substituted compound $Cu_{10}Ni_2Sb_4S_{13}$ in Figure S4 of the ESI. In our study we assume a ferromagnetic (FM) configuration of the magnetic moments since our calculations for $Cu_{10}Ni_2Sb_4S_{13}$ predict that the antiferromagnetic (AF) spin alignment is 0.1 eV higher in energy than FM. Since the Ni 3*d* states are only slightly higher in energy than the Cu 3*d* states, it can be expected that they will strongly hybridize with the valence bands of the host. The majority spin $e_g$ and $t_{2g}$ states of nickel indeed lie in the same energy range as the Cu 3*d* states and are fully occupied (upper panel of Figure 2). In the minority spin channel, however, three partially empty acceptor-like bands exist above the Fermi level (lower panel of Figure 2), but these bands overlap with the filled valence bands of the host and there is a finite eDOS at the Fermi level. The total spin is found to be 3/2 per formula unit of $Cu_{11}Ni_1Sb_4S_{13}$, giving $S(S+1)=3.75$ in good agreement with the effective magnetization values of 3.6 deduced from magnetic susceptibility measurements by Suekuni *et al.*[20]. Our results for the double-substituted $Cu_{10}Ni_2Sb_4S_{13}$ compound in Figure S4 of the ESI show that the band structures of $Cu_{11}Ni_1Sb_4S_{13}$ and $Cu_{10}Ni_2Sb_4S_{13}$ differ by the existence of an additional partially empty minority spin band at the Fermi level, giving a total spin $S$=2.

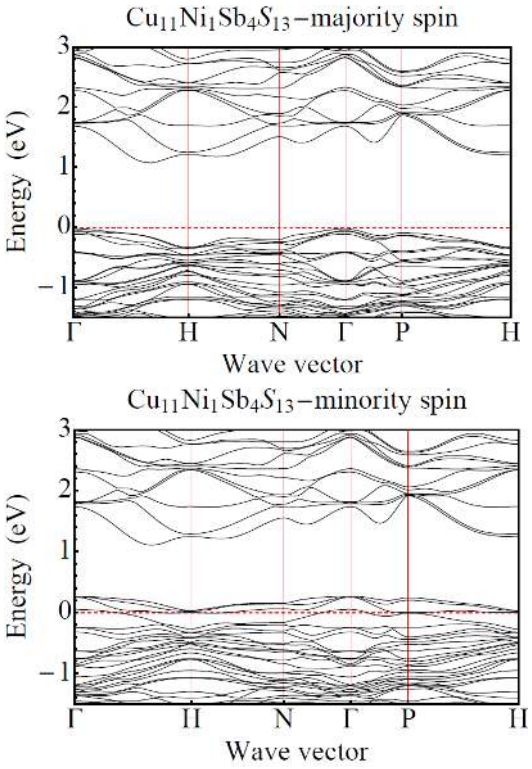


Figure 2. Electronic band structure of $Cu_{11}NiSb_4S_{13}$. While the majority spin states are fully occupied (upper panel), three partially occupied bands exist at the Fermi level in the minority spin channel (lower panel).

Analysis of the partial eDOS curves of the Ni-substituted compounds (see Figure 3 and Figure S5 of the ESI) shows that the partially empty bands are formed by hybridizing Ni 3*d* states with the *p-d* hybridized valence bands of the host. Since the number of holes per formula unit varies from 2 for the pure compound ($x$=0), to 3 for $x$=1, and to 4 for $x$=2, this suggests that each substitutional Ni introduces an additional hole state into the VB of the host. At all Ni concentrations considered, the resulting band structure remains metallic, in agreement with the experimental results of Suekuni *et al.* [6,7] on Ni-doped tetrahedrite. For comparison, Fe in tetrahedrite acts like a regular dopant whose main effect is to shift the Fermi level, in agreement with experimental measurements.[5] We found earlier[5] that iron impurities in tetrahedrite are in the high-spin $Fe^{3+}$ $d^5$ configuration (total spin S=5/2) because strong exchange splitting pushes the minority $e_g$ and $t_{2g}$ orbitals above the Fermi level and into the band gap. At Fe concentrations $x$=1, all VB holes are filled and the compound becomes electrically insulating, while optimal thermoelectric performance is achieved near $x$=0.5[5] Here we hypothesize that further optimization of Ni-doped tetrahedrite may be achieved by re-adjusting the Fermi level close to the top edge of the valence band by addition of Zn and filling the holes introduced by Ni substitution.

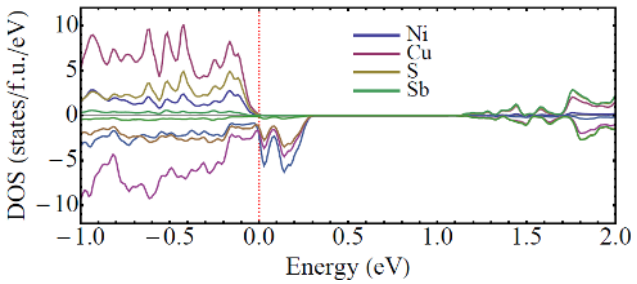


Figure 3. The partial electron density of states of $Cu_{11}NiSb_4S_{13}$. The bands above the Fermi level (shown as a dotted vertical line) are formed by hybridizing Ni 3*d*, Cu 3*d*, and S 3*p* orbitals.

Before describing our experimental results on Zn codoping, we address the question of the valence state of the dopant nickel ions. While one could expect the Ni ions to be in the $Ni^{2+}$ valence state and the electronic $d^8$ configuration, our calculations are consistent with the interpretation that nickel adopts a monovalent $Ni^{1+}$ $d^9$ configuration with a local spin of S=1/2. This interpretation is supported by several facts. First, the Ni 3d states are only slightly higher in energy than the Cu 3d states. Since the latter form the top of the tetrahedrite VB, on general grounds one should not expect a strong charge transfer from the Ni 3d orbitals to the VB of the host. Second, the appearance of a hole for each substitutional Ni (see above) is consistent with the $d^9$ valence configuration. Third, the change in the total spin from S=3/2 in $Cu_{11}NiSb_4S_{13}$ to S=2 in $Cu_{10}Ni_2Sb_4S_{13}$ shows that the second nickel ion has a local spin moment of S=1/2, which is only compatible with the $d^9$ configuration. The higher total spin value of S=3/2 value in $Cu_{11}NiSb_4S_{13}$ can be attributed to induced magnetic moments on the neighboring sulfur and copper atoms due to band hybridization and ferromagnetic exchange coupling with the Ni dopant. Fourth, integration of the spin density in an atomic sphere of radius 0.1286 nm around Ni gives a local moment value of S=1/2; this result is also supported by the analysis of the eigenvalues and eigenvectors of the PAW density matrix. Finally, the results of the Bader charge analysis, which does not depend on the somewhat arbitrary choice of the ionic radii and PAW augmentation spheres, are given in Table S1 of the ESI. It is seen that the Bader charge of nickel in $Cu_{11}NiSb_4S_{13}$ is 9.43, while that of the tetrahedrally coordinated Cu is 10.5. Since the copper ions are in the closed shell d10 configuration, this provides strong support that nickel ions are in the monovalent $Ni^{1+}$ $d^9$ state.

In order to shed further light on this issue, we have also calculated the band structure of $Cu_{10}ZnNiSb_4S_{13}$ (Figures S6 and S7 of the ESI) and measured the magnetic susceptibility of $Cu_{10}Zn_2Sb_4S_{13}$, $Cu_{10}ZnNiSb_4S_{13}$, and $Cu_{10}Ni_2Sb_4S_{13}$ (Figures S8 and S9 of the ESI). For $Cu_{10}ZnNiSb_4S_{13}$ we find from band structure calculation a total spin of S = 1 per Ni ion; again the Ni itself has a local moment of S = ½ with the remainder induced on the neighboring Cu and S atoms. Our susceptibility measurements show that the $Cu_{10}Zn_2Sb_4S_{13}$ compound is diamagnetic over most of the temperature range, as expected for an undoped semiconductor, while for both $Cu_{10}ZnNiSb_4S_{13}$ and $Cu_{10}Ni_2Sb_4S_{13}$ we find a total spin of S = 1 per Ni ion. While at first glance this value is consistent of a valence of $Ni^{2+}$, in fact, we can only reconcile this observation with the band structure calculations as well as the observation that both $Cu_{10}ZnNiSb_4S_{13}$ and $Cu_{10}Ni_2Sb_4S_{13}$ are metallic and not insulating if we have a valence state $Ni^{1+}$ with a local moment of S = ½ on each Ni ion, with the remaining spin ½ moment induced on the neighboring Cu and S. While $Ni^{1+}$ may be an unusual charge state for Ni in molecules and ionic crystals, one must use caution when assigning valence to impurities in partially covalently bonded solids where impurity orbitals can easily hybridize with the electronic states of the host. In fact, the $Ni^{1+}$ state is known to occur for Ni in tetrahedral coordination as a dopant in II-VI and III-V semiconductors such as ZnS[21], GaP[22], and GaAs[23], chemical environments very similar to that of Ni in tetrahedrite. The question of magnetism in tetrahedrites is a very interesting one that is beyond the scope of this paper, but is deserving of a deeper investigation using more sensitive local probes such as electron paramagnetic resonance or x-ray absorption, which will be the subject of a future study.

**Electrical Properties.** In order to test our hypothesis, we begin with a Ni doping level yielding the highest *zT*, $Cu_{10.5}Ni_{1.5}Sb_4S_{13}$, and progressively substitute Zn for Cu. Figure 4 shows the temperature dependence of the electrical transport properties of $Cu_{10.5}Ni_{1.5-x}Zn_xSb_4S_{13}$ ($x$ = 0, 0.2 0.5, and 1). As shown in the upper panel, the electrical

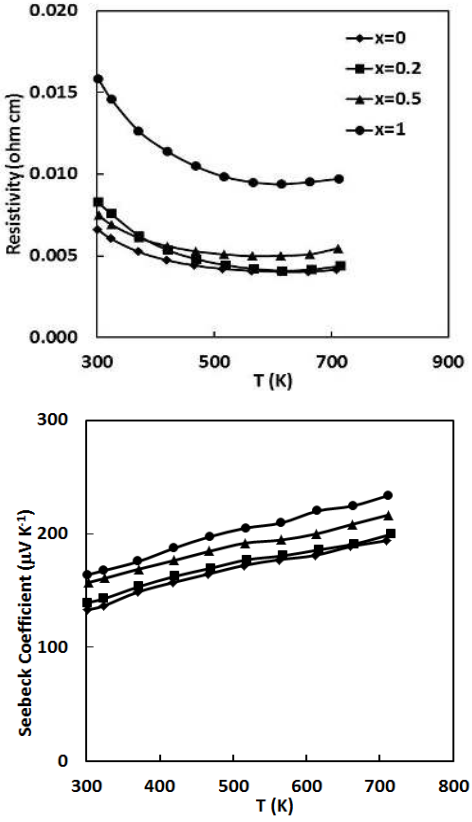

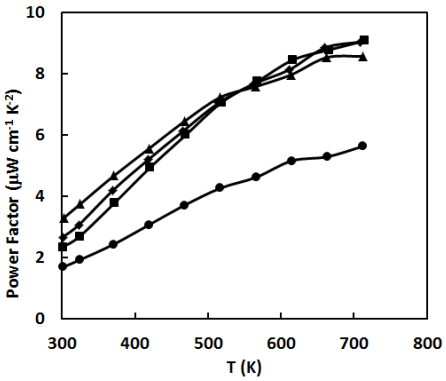


Figure 4. Electrical transport properties of $Cu_{10.5}Ni_{1.5-x}Zn_xSb_4S_{13}$ tetrahedrites. The electrical resistivity (upper) and Seebeck coefficient (center), both increase with Zn addition as electrons fill empty holes in the valence band. Although the resistivity is increased with Zn doping, the thermoelectric power factor (lower) remains unchanged up to x = 0.5.

resistivity of these samples decreases weakly until the mid-temperature region, and then rises at higher temperature. This behavior is consistent with a highly degenerate semiconductor or weakly metallic system with low carrier mobility. The same behavior has been observed in Zn-doped samples. For the $x$ = 0 sample ($Cu_{10.5}Ni_{1.5}Sb_4S_{13}$), the resistivity at 723 K is $4.1 \times 10^{-3}$ ohm cm, much lower than that of $Cu_{10.5}Zn_{1.5}Sb_4S_{13}$, which has a resistivity of $1.2 \times 10^{-2}$ ohm cm. This can be explained by the spin splitting of the Ni $t_{2g}$ states as discussed above for Figure 1. After adding a small amount of Zn ($x$ = 0.2 and 0.5) into $Cu_{10.5}Ni_{1.5}Sb_4S_{13}$, the resistivities are increased by 6% and 30%, respectively. At $x$ = 1, the resistivity becomes two times larger than that of the $x$ = 0 sample. The additional electrons from Zn fill the holes in the valence band, moving the Fermi level closer to the top of the valence band and decreasing the carrier density. In order to tune the Seebeck coefficient, the optimum position of the Fermi level should be close to the band edge where a large energy dependence of the electronic DOS can be obtained. The center panel of Figure 4 displays the temperature dependence of Seebeck coefficients: for the three co-doped samples, the Seebeck coefficients are all increased, as we expect.

In order to determine the optimal position of the Fermi level, we estimated the reduced Fermi energy by using a single parabolic band model with acoustic phonon scattering as the predominant scattering mechanism. Then[24]:

$$S = \pm\frac{k_B}{e}\left(2\frac{F_1(\eta)}{F_0(\eta)} - \eta\right), \qquad (1)$$

where $k_B$, e, $\eta$ are the Boltzmann constant, electron charge, and the reduced Fermi energy, respectively, and $F_n$ is a Fermi integral of order $n$. The Fermi energy moves closer to the top of the valence band with increasing Zn content, and at high temperatures even moves slightly into the gap. The power factor for all samples is displayed in lower panel of Figure 4. Due to the enhancement in Seebeck coefficients, the power factors of the $x$ = 0.2 and $x$ = 0.5 samples are changed hardly at all although their resistivities increase during Zn co-doping.

**Thermal conductivity and figure of merit.** Figure 5 (top panel) shows the total thermal conductivity as a function of temperature for all $Cu_{10.5}Ni_{1.5-x}Zn_xSb_4S_{13}$ samples ($x$ = 0, 0.2 0.5, 1) together with pure $Cu_{12}Sb_4S_{13}$ and $Cu_{10}Zn_2Sb_4S_{13}$ for comparison. The total thermal conductivity of all samples increases with increasing temperature due to an increased electronic contribution – with the exception of $Cu_{10}Zn_2Sb_4S_{13}$, which is almost insulating and thus has a negligible electronic contribution. Pure $Cu_{12}Sb_4S_{13}$ has a total thermal conductivity in the range of 1.2 W/(m K) to 1.5 W/m K from room temperature to high temperature, while the total thermal conductivities of all the other samples are below 0.8 W/(m K) due to reduction in both electronic and lattice contributions. In order to clarify the effect of Ni and Zn co-doping on the lattice thermal conductivity, we subtract the electronic thermal conductivity obtained by applying Wiedemann-Franz law from total thermal conductivity:

$$\kappa_e = LT/\rho, \qquad (2)$$

where $L$ is the Lorenz number and $\rho$ is electrical resistivity. The Lorenz numbers are calculated[24] using the following expression:

$$L = \frac{k_B^2}{e^2}\frac{3F_0(\eta)F_2(\eta) - 4F_1^2(\eta)}{F_0^2(\eta)}, \qquad (3)$$

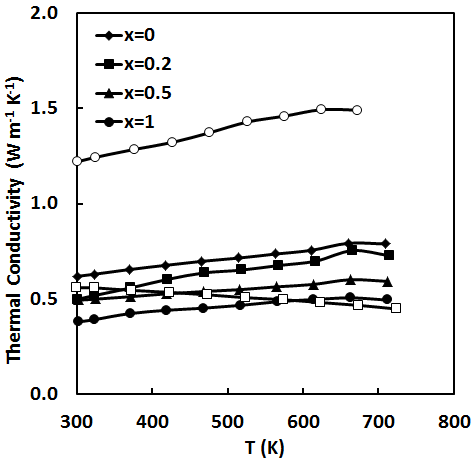


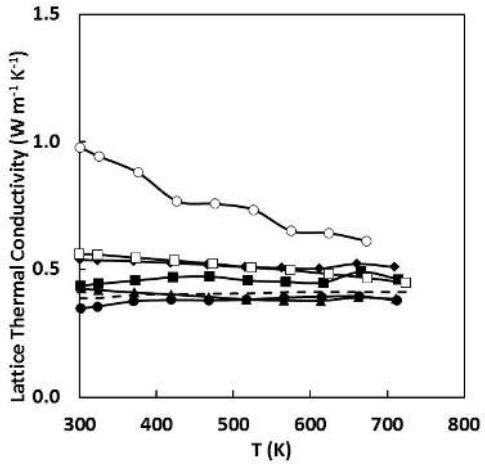

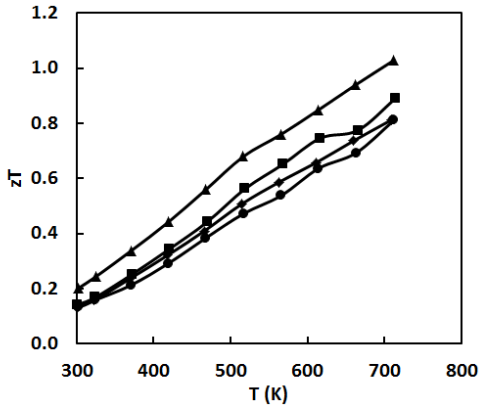


Figure 5. Total (upper) and lattice (center) thermal conductivity of $Cu_{10.5}Ni_{1.5-x}Zn_xSb_4S_{13}$ tetrahedrites. The open circles are for pure $Cu_{12}Sb_4S_{13}$, the open squares for $Cu_{10}Zn_2Sb_4S_{13}$, and the dashed line represents the minimal thermal conductivity of tetrahedrites, calculated from the kinetic formula assuming a phonon mean free path equal to the interatomic distance. In the co-doped samples, the lattice thermal conductivity approaches this minimum value. This, combined with the near constant power factor, gives rise to an increase in thermoelectric figure of merit (lower).

and employing the reduced Fermi energy values found previously from the Seebeck data. The calculated Lorenz numbers for all co-doped samples are in the range of $1.8 \times 10^{-8}$ to $1.6 \times 10^{-8}$ W Ω /K² from room temperature to high temperature, significantly lower than the metallic limit of $2.45 \times 10^{-8}$ W Ω /K². Using these calculated Lorenz numbers, we determine the lattice thermal conductivity by subtracting the electronic contribution from the total: the results are shown in the middle panel of Figure 5. The theoretical minimum lattice thermal conductivity estimated by formula $k_{min} = \frac{1}{3} C_v v l$ , where $l$ is the minimum phonon mean free path, is also shown as dashed line. For the latter estimate we use the specific heat $C_v$ data obtained from our experiments and a mean sound velocity $v = 2500$ m/s estimated from elastic properties measurements[13]. The minimum phonon mean free path is on the order of one phonon wavelength, which is approximately the interatomic distance[25] $l$ = 0.226 nm[26]. The lattice thermal conductivity of pure $Cu_{12}Sb_4S_{13}$ decreases from 1.0 W/m K to 0.6 W/m K with increasing temperature, following a $T^{-1}$ law, where the phonon mean free path exceeds the interatomic distance. Therefore, the lattice thermal conductivity of pure $Cu_{12}Sb_4S_{13}$ is close to but still above the theoretical minimum value of about 0.4 W/(m K). As we have pointed out previously[5], the anharmonicity in the tetrahedrite structure leads to the intrinsic low thermal conductivity. Here, we find that the dopant atoms (Ni and Zn) replacing Cu atoms in tetrahedrites further decrease the lattice thermal conductivity through solid solution point defect phonon scattering, pushing the lattice thermal conductivity down close to theoretical minimum. The lattice thermal conductivity of all the doped samples is temperature independent throughout the measured temperature range. The single element doped sample, $Cu_{10}Zn_2Sb_4S_{13}$ in which both of the two available Cu atoms are replaced by Zn atoms, exhibits a lattice thermal conductivity of 0.45 W/(m K).

By combining the electronic transport and thermal conductivity data, the overall figure of merit ($zT$) values are computed, and the results are shown in the lower panel of Figure 5. By addition of Zn to $Cu_{10.5}Ni_{1.5}Sb_4S_{13}$, $zT$ can be enhanced from 0.81 to 0.99 and 1.03 for $x$ = 0.2 and $x$ = 0.5, respectively.

## CONCLUSION

In summary, with optimum Fermi energy level and minimum lattice thermal conductivity, the $zT$ value of tetrahedrite co-doped with Ni and Zn rises to above unity at 723 K, making this material one of the best $p$-type TE materials in this temperature region. Considering the low cost and earth abundant nature of tetrahedrites, this class of materials should be a good candidate for large scale thermoelectric applications.

## AUTHOR INFORMATION

### Corresponding Author

*(D.T.M.) email: dmorelli@egr.msu.edu

### Author Contributions

The manuscript was written through contributions of all authors. All authors have given approval to the final version of the manuscript.

## ACKNOWLEDGMENT

This work was supported as part of the Center for Revolutionary Materials for Solid State Energy Conversion, an Energy Frontier Research Center funded by the U.S. Department of Energy, Office of Science, Office of Basic Energy Sciences under Award Number DE-SC0001054. We used computing resources at the National Energy Research Scientific Computing Center, which is supported by the US DOE under Contract No. DE-AC02-05CH11231.

**SUPPORTING INFORMATION:** This information is available free of charge via the Internet at http://pubs.acs.org/.

## REFERENCES

(1) Slack, G.A. *CRC Handbook of Thermoelectrics*, ed. D.M. Rowe, CRC Press, Boca Raton, FL (1995)

(2) Biswas, K., He, J., Blum, I.D.,, Wu, C.-I., Hogan, T.P., Seidman, D.N., Dravid, V.P., and Kanatzidis, M.G. *Nature* **2012**, 489, 414

(3) Liu, H., Shi, X., Xu, F., Zhang, L., Zhang, W., Chen, L., Li, Q, Uher, C., Day, T., and Snyder, G.J., *Nat. Mater.*, **2012**, 11, 422

(4) Dennler, G., Chmielowski, R., Jacob, S., Capet, F., Roussel, P., Zastrow, S., Nielsch, K., Opahle, I., and Madsen, G.K.H. *Adv. Energy Mater.* 2014, 4, 1301581

(5) Lu, X., Morelli, D.T., Xia, Y., Zhou, F., Ozolins, V., Chi, H., and Uher, C. *Advanced Energy Materials* **2012**, *3*, 342

(6) Suekuni, K., Tsuruta, K., Ariga, T., and Koyano, M. *Applied Physics Express* **2012**, 5, 05120

(7) Suekuni, K., Tsuruta, K., Kunii, M., Nishiate, H., Nishibori, E., Maki, S., Ohta, M., Yamamoto, A., and Koyano, M. *Journal of Applied Physic*s **2013**, *113,* 043712

(8) Heo, J., Laurita, G., Muir, S., Subramanian, M.A., and Keszler, D.A., *Chem. Mater.* **2014**, *26*, 2047

(9) Wuensch, B.J., *Zeitschrift fur Kristallographie* **1964**, 119, 437

(10) Skoug, E.J. and Morelli, D.T. *Physical Review Letters* **2011**, *107*, 235901

(11) Lu, X. and Morelli, D.T. *Physical Chemistry Chemical Physics* **2013**, *15*, 5762

(12) Lu, X. and Morelli, D.T. *MRS Communications*, **2013**, *3*, 12

(13) Fan, X., Case, E.D., Lu, X., and Morelli, D.T. *Journal of Material Science* **2013**, *48*, 7540

(14) Kresse, G., and Hafner, J. *Physical Review B* **1993**, *47,* 558

(15) Kresse, G., and Hafner, J. *Physical Review B* **1994**, *49*, 14251

(16) Kresse, G., and Furthmüller, J. *Physical Review B* **1996,** *54,* 11169

(17) Kresse, G., and Furthmüller, J. *Comput. Mater. Sci.* **1996,** *6*, 15

(18) Perdew, J.P., Burke, K., and Ernzerhof, M. *Physical Review Letters* **1996,** *77,* 3865

(19) Perdew, J.P. Burke, K., and Ernzerhof, M. *Physical Review Letters* **1997,** *78,* 1396

(20) Suekuni, K., Tomizawa, Y., Ozaki, T., and Koyano, M. *Journal of Applied Physics* **2014**, 115, 143702

(21) Waldmann, H., Mahnke, H.-E., Spellmeyer, B., Sulzer, G., Zeitz, W.-D., Hoffmann, H., and Gumlich, H.-E. *Nuclear Instruments and Methods in Physics Research B* **1992**, 63, 221

(22) Kaufmann, U., Koschel, W. H., Schneider, J., and Weber, J. Physical Review B **1979**, 19, 3343

(23) Ennen, H. Kaufmann, U., and Schneider, J., Solid State Communications **1980**, 34, 603

(24) Fistul, V.I. *Heavily Doped Semiconductors,* Plenum, New York, **1969**

(25) Slack, G.A. in *Solid State Physics* (ed. F. Seitz, D. Turnbull, and H. Ehrenreich, Academic Press, New York, **1979**, Vol. 34, p. 1

(26) Pfitzner, A., Evain, M., and Petricek, V. *Acta Crystallographica* **1997**, *B53*, 337

Table of Contents Figure: